Simulation of near-field dispersion of pollutants using detached-eddy simulation[☆]

M. Lateb[a,*], C. Masson[a], T. Stathopoulos[b], C. Bédard[a]

[a] *Department of Mechanical Engineering, École de technologie supérieure (Éts) 1100 Notre-Dame West, Montreal, H3C 1K3 Canada*
[b] *Department of Building, Civil and Environmental Engineering, Concordia University 1455 de Maisonneuve Blvd. West, Montreal, H3G 1M8 Canada*

Abstract

A numerical simulation is developed using the unsteady-state turbulence model on a structured highly refined grid to predict the wind-flow field and dispersion field of a pollutant emitted from a rooftop stack around a two-building configuration. The results obtained are compared with those of a steady-state model previously reported by the authors. The pollutant concentrations are examined on the roof where the stack is located as well as on the leeward wall of an upstream tower to the emitting building in order to evaluate how the pollutant is dispersed by the DES model compared to RNG model. DES results are discussed against those from RNG $k-\epsilon$ approach and wind tunnel. The study emphasizes limits in reproducing correctly the wind flow and dispersion fields due to underestimation and/or overestimation of the Reynolds stress components and the steady-state methodology when using the RNG $k-\epsilon$ model. Despite such limits, the RNG model produces a similar average error, in terms of concentrations, to that obtained with the DES model.

Keywords: Computational fluid dynamics (CFD), Detached-eddy simulation (DES), Pollutant dispersion, Roof stack emissions, RNG $k-\epsilon$ turbulence model, Two-building configuration

1. Introduction

Pollution in the atmospheric boundary layer (ABL) is an important environmental problem which affects human health. Investigations of pollutant transport and dispersion have received a lot of attention in recent years, and become a focal point in environmental research because of the increasing interest for protecting air quality [1]. Besides, this subject is of great concern especially in the urban environment when the crucial issues of well-being and human comfort are considered.

Turbulent wind flows have long presented a considerable obstacle to the accuracy and applicability of calculations in industrial applications [2]. The types of flows encountered in the field of wind engineering are no exception, and consist of many complex flow features which may contain recirculation zones and stagnation points [3]. Indeed, in the lower atmospheric boundary layer, specifically in cities around individual and/or groups of buildings, the superposition and interaction of the flow patterns induced by buildings and structures strongly affect the dispersion and govern the movement of pollutants [4]. Therefore, complicated and highly unpredictable dispersion phenomena are created. Clearly, understanding the process of pollution dispersion and its mechanisms still remains a great challenge for wind engineering researchers. Nonetheless, the scientific community has significantly contributed

[☆] This work is an extended version of a paper presented at the 12th Americas Conference on Wind Engineering (12ACWE), Seattle, WA, June 16−20, 2013.

[*] Corresponding author. Tel.: +1 514 396 8800 ext. 7838; fax: +1 514 396 8530.
Email address: Mohamed.Lateb@etsmtl.ca; Mohamed.Lateb@gmail.com (M. Lateb)

to daily life quality by controlling and maintaining air quality in buildings and offices within the acceptable norms typically established and authorised by governments and/or professional organizations [5].

Substantial research projects have been carried out and are available in the literature on the topic of pollutant dispersion. They have used a wide range of different methods (e.g. field tests, laboratory modelling, semi-empirical methods and numerical approaches) to evaluate pollutant dispersion, identifying their advantages and disadvantages [6]. During the past years, especially in urban environments, pollutant dispersion has been studied extensively by means of both experimental and numerical approaches. Field measurements (e.g. [7, 8]), wind tunnel testing (e.g. [9–13]), semi-empirical methods (e.g. [14, 15]) and numerical modelling (e.g. [16–20]) have been performed, on the one hand to get an insight into the physical pollution processes, and on the other hand, to obtain a better comprehension of the coupled mechanisms occurring around buildings and/or cluster of buildings. Among these methods, numerical modelling with computational fluid dynamics (CFD) appears as one of the most accessible and largely spread approach to study wind environmental problems because of the lower costs, the advantages and reliability of such approach. However, CFD simulations are not straightforward to perform and their results still require validation to establish extended acceptability [21]. Therefore, the need of validating numerical studies makes the experimental tests necessary.

Notwithstanding the widespread use of CFD studies, the quality of results depends mainly on many physical and numerical parameters which can compromise accuracy and reliability. From that point of view, many authors and organizations have developed practice guidelines (e.g. [22–30]) to establish a common methodology for verification and validation of CFD simulations in certain cases, and/or to assist and support the users in making a better implementation of CFD in other cases. In addition to the fundamental error of selecting an inappropriate physical model to simulate a flow field (i.e. steady or unsteady approach), there are basically two types of difficulties that can produce erroneous results in CFD [30]: (i) modelling errors (e.g. turbulence models and physical boundary conditions) and (ii) numerical approximation errors (e.g. grid design, discretization scheme and iterative convergence).

Regarding turbulence modelling errors, various turbulence models (i.e. steady Reynolds−averaged Navier−Stokes (RANS), unsteady RANS (URANS), large-eddy simulation (LES) and hybrid URANS/LES) reported in the literature are well known to the computational wind engineering (CWE) community, as they have been listed by many authors (e.g. [27, 6]). Several studies have investigated and assessed the performance of such different turbulence models to predict the flow field around buildings (e.g. [31, 32]). However all studies agree on the difficulty of some models and the differences between the various approaches to reproduce the complex and random character of the flow field. In addition, the dispersion field is closely related to the overall behaviour of the wind flow as stated by Tominaga and Stathopoulos [33]. Therefore, the choice of the turbulence model is revealed crucial to reproduce an accurate dispersion process, and, consequently, essential to understand the pollutant transport mechanisms.

The present study follows previous work of Lateb et al. [34] where various RANS $k-\epsilon$ turbulence models were compared (i.e. standard $k-\epsilon$, re-normalized group $k-\epsilon$ and realizable $k-\epsilon$ referred to as SKE, RNG and RLZ throughout, respectively). Previous work suggested that the limitations in RANS models to reproduce the experimental results are probably due to an incorrect estimation of Reynolds stress components and the steady-state methodology of the tested models. Thus, the purpose of this study is to reproduce the flow and dispersion fields compared to the RANS approach using Fluent software. The detached-eddy simulation (DES) – referred as the most widely known hybrid URANS/LES by Franke et al. [27] – has been selected for the present study because of the well established limitations of the two following models in resolving the internally induced fluctuations of flow and concentration fields [35], i.e. the high computational cost of LES and the low accuracy of URANS. For more details about the technique, advantages and applications of the DES approach, the reader can refer to works existing in the literature (e.g. [36–47]).

In this work, one case is considered because of the long time required by DES modelling. Regarding the objectives of this work cited above, the most critical case is selected, namely when the pollutant is emitted at high speed from the stack (i.e. $h_s = 1$ m and $M = 5$, where h_s is the stack height and M

the momentum ratio which represents the ratio between the exhaust velocity of the pollutant w_e and the wind velocity U_H at the height of the BE building). Such case induces complex pollutant/flow-field interactions above the stack. Consequently, the capability of the DES model to reproduce the dispersion process is severely tested. It is worth noting that among the various RANS $k-\epsilon$ models tested by Lateb et al. [34], the RNG $k-\epsilon$ model provided the best agreement with the wind tunnel results conducted by Stathopoulos et al. [48] for the current considered case ($h_s = 1$ m and $M = 5$). DES results are thus compared with those from the RNG approach and wind tunnel experiments.

The paper is organized as follows. Section 2 summarizes the computational details including the DES concept, the grid generation, the boundary conditions and the solution strategy. Section 3 demonstrates the consistency of both constructed grid and statistical averaging period. The results are described and compared to those of the RNG $k-\epsilon$ model and experimental data in section 4. The analysis and discussion of results are presented in section 5. Finally, the main findings of the study are summarized in section 6.

2. Computational details

2.1. Detached-eddy simulation model

The strategy of DES model is such that switching from URANS to LES models is realised according to mesh definition and not to the local turbulent properties of the flow [49]. Thus the turbulent viscosity obtained depends on the local grid spacing, Δx_i, and the sub-grid scale (SGS) stresses are parameterized using a turbulent viscosity model. The RLZ turbulence model is selected to calculate the turbulent viscosity for both strategies (i.e. as URANS model in boundary layer regions and LES sub-grid scale model in massive separated regions) since the RLZ model is the only model available in Fluent among the various RANS $k-\epsilon$ models tested by Lateb et al. [34]. In addition to the continuity and momentum equations, two others are added to estimate the turbulent viscosity, ν_t, at each cell. One equation for the turbulent kinetic energy, k, another for the turbulent dissipation rate, ϵ, and their detailed expressions can be found in work of Lateb et al. [50].

2.2. Grid generation

Since the present research is complementary to Lateb et al. [34] work, the same site is used. Therefore, the reader can refer to that work for more details about the configuration and the dimensions of the two buildings. The main difference in the grid generation of these two studies is the grid refinement required by this unsteady three-dimensional approach particularly in the separated flow regions where the LES model is used. The "wall function" is used as near wall treatment for the present study since it is the only approach available when using DES model. Basically, there are two overlapping layers over walls: an inner layer where viscous processes dominate, and an outer layer far from these effects [18]. The near wall treatment used bridges the viscosity-affected region between the wall and the fully turbulent region; therefore, on the one hand a substantial refinement of grid meshing is saved, and on the other hand the attached boundary layer regions are assured to be modelled by the URANS model.

The process of refining the grid deals with three criteria. The spacing cells, Δx_i, should (i) be fine enough near wall regions to capture the high gradients which occur within the turbulent boundary layer, and to reach the slope $-5/3$, associated with the range of frequencies in which the energy cascade is dominated by the inertial transfer, (ii) be smaller than the turbulence length scales, defined previously as $l_{rke} = k^{3/2}/\epsilon$, to make sure that the separated flow regions will be treated by the LES approach out of the turbulent boundary layer, and (iii) keep the spacing length perpendicular to each wall at least equal or larger than the two other spacing directions to eliminate the gray zone and thus avoiding a modelled-stress depletion (MSD) defined and noticed by Spalart et al. [51].

Starting from the grid used in Lateb et al. [34] and the results obtained with the steady RLZ model solution, Taylor microscale $l_\lambda = (10\nu k/\epsilon)^{1/2}$ is evaluated using the k and ϵ parameters in several planes along x, y and z directions [52]. Note that l_λ is always much smaller than l_{rke} [53].

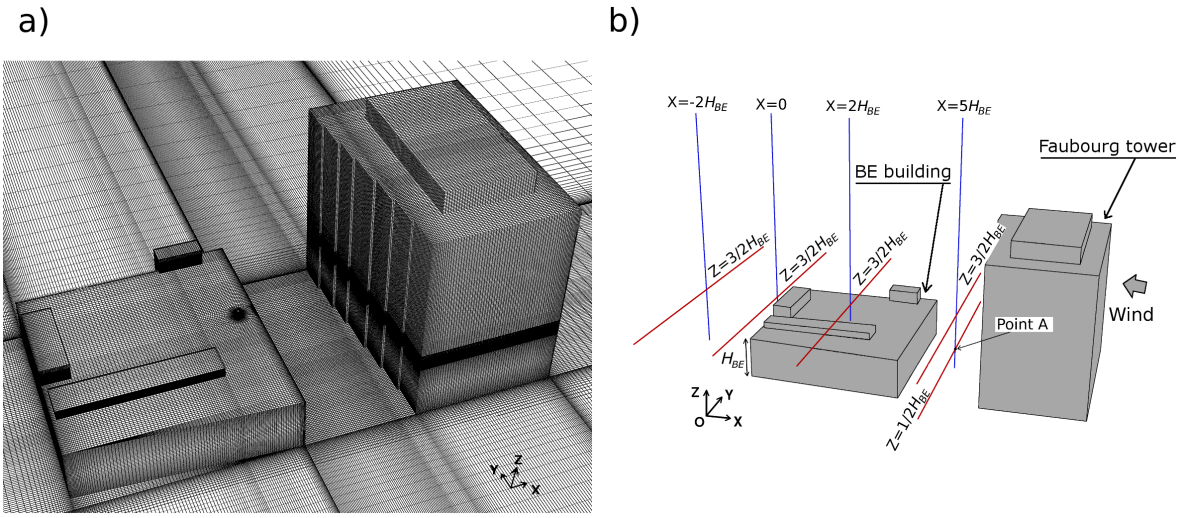

Figure 1: The two-building configuration showing (a) the highly refined meshing and (b) various positions of horizontal and vertical lines evoked in the present study. Note that the origin of the reference frame is located at the base of the wall downstream of the BE building at its centre, and the wind blows in the negative x direction.

As a grid refinement study was already conducted for that grid (see Lateb et al. [54]), the l_λ values evaluated remain approximately the same at each cell even with a further refined grid. Afterwards the smallest l_λ value found is taken as a benchmark for the spacing grid near solid walls in the three directions, and the stretching ratio is kept equal to 1 in the entire regions near walls, above the BE building roof and between the two buildings to respect the criterion (iii). It is worth noting that the grid is composed by hexahedral cells, hence only one refining is required for each direction. The spacing cells in these regions is set under the turbulence length scale benchmark to make sure that, out of the boundary layer regions, the inequality $l_{rke} \gg l_{les}$ is respected so that the switch to LES approach can occur. Therefore, the criteria (i) and (ii) are taken into account. Elsewhere, far from the near walls and between the two buildings, the stretching ratio is extended to 1.1 to respect the commonly recommended value of 1.3 [28]. Finally, the grid obtained for the unsteady DES simulations is composed of about 11 million cells spread over 321×177×194 cells in x, y and z directions, respectively. Fig. 1 shows the neighbourhood of the two buildings of concern as a general view of the highly refined new grid, and the various positions of the vertical and horizontal lines evoked in the following sections.

2.3. Boundary conditions

After the converged solution obtained on the new grid (i.e. 11 million of cells) using the steady-state RLZ $k-\epsilon$ turbulence model with the same boundary conditions as those used by Lateb et al. [34], a spectral synthesizer method, based on the random flow generation technique originally proposed by Kraichnan [55] and modified by Smirnov et al. [56], is imposed at the domain inlet to generate fluctuating velocity components with a Fourier harmonics number set to 100. The number of 100 is considered as the minimum threshold of large numbers [57], and it is desirable to use the minimum number of harmonics since large numbers increase the computational cost [58]. The exit of the domain is referred as an outflow boundary condition, which assumes no velocity gradient in the exit direction, since the exit plane is sufficiently far from the two buildings wake region. Symmetry condition, which implies zero normal velocity and zero normal gradients for all variables, is used at the top of the domain. For the side boundaries, periodic conditions are imposed to capture correctly the vortex shedding which can occur on these planes. The equations are discretized in time by using a second-order fully implicit scheme, and then iteratively solved using the segregated solver, for which the SIMPLE (Semi-Implicit Method for Pressure-Linked Equations) algorithm [59] is used to derive

the pressure-correction equations. The convection terms are discretized using a second-order upwind scheme, whereas for the momentum equations a second-order central difference scheme is used. All walls of the two buildings are assumed to be smooth by using no-slip condition. At the ground level, no particular treatment is assigned and the wall roughness is not taken into account. In addition, the length of the domain upstream of the buildings is short enough to limit the horizontal inhomogeneity affecting the inlet profiles. Note that this boundary condition at the ground surface is inspired from works of Gousseau et al. [60, 61].

2.4. Solution strategy

Primary circulation is carried out to reach the establishment of the flow field to remove the influence of the initial conditions before averaging to get statistically-steady values. Time scale of these first simulations is evaluated by the residence time of a single particle crossing through the whole computational domain. The calculated time, noted t, results in a value of about 1 second. The time step, Δt, is chosen by consideration of the Courant−Friedrichs−Lewy (CFL) number [62] which assures the balance of the temporal and spatial scales when it is kept around 1 [63]. It is worth noting that a small time step is recommended for the accuracy of the results [38]. For a possible approach of CFL concept (i.e. to obtain a CFL value as close as possible to 1 in the entire domain), the value of the CFL number is set to 0.5 in the evaluation of the time step. Finally, a time step of 1×10^{-4} s is obtained. It gave a maximum CFL number of approximately 1.2 with smaller values than 1 in 99% of the cells. The time is non-dimensionalized by U_H and H_{BE} and the flow is averaged, after the primary circulation, during $T = 400$ non-dimensional time units ($t^* = tU_H/H_{BE}$) which represents 40 000 time steps (Δt). Note that H_{BE} and U_H are the BE building height and the particle velocity estimated at H_{BE}, respectively. For more details, the reader is referred to works of Lateb [64].

3. Consistency of DES simulations

Fig. 2 depicts the time history data of velocity components, u_i, recorded at point A located in the centreline ($y = 0$) between the two buildings as illustrated in Fig. 1b. No periodic fluctuation is clear for all velocity components, therefore this fact highlights the random and unpredictable characteristics of the flow behind the tower. The latter provides an idea about the large mixing that occurs in that region.

3.1. Grid consistency

Plots of power spectral density (PSD) using a fast Fourier transform (FFT) algorithm, corresponding to velocity components depicted in Fig. 2, are shown in Fig. 3. The velocity component data are recorded at the same point A. The curves represent the energy cascade which develops from large to small scales [19]. The cascade phenomenology for the energy transfer takes its origin from the large structures that break down into smaller structures and so on. The latter in turn, tend to a universal and isotropic structure more or less independent of the large scales [16]. The phenomenon occurs mainly in the massively separated regions where the dominant unsteady structures are resolved by LES modelling. The end of the cascade is controlled by the filter width which activates the SGS model [65]. The range of frequencies associated with the inertial transfer during the energy cascade is clearly reached as shown in Fig. 3 by the slope $-5/3$. Therefore, the consistency of the constructed grid is demonstrated and justified.

3.2. Statistical averaging period consistency

To ensure that the averaging period used to obtain statistical values is sufficiently acceptable, the average error, e_a, for simulated and experimental values of non-dimensional concentration, K, at various samplers located on the BE building roof and the top of the Faubourg tower leeward wall

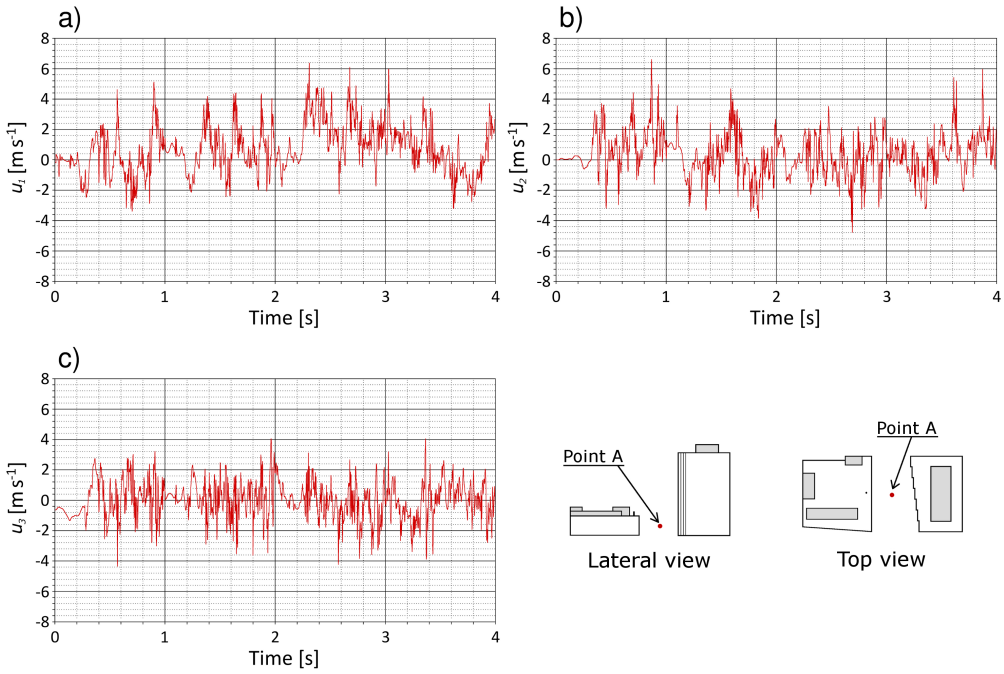

Figure 2: Time history curves of velocity components, u_i, in (a) streamwise, (b) spanwise, and (c) vertical directions, recorded at point A located in the centreline between the two buildings and at half-height of the BE building from the ground (i.e. $y = 0$ m, $x = 5H_{BE}$ and $z = 1/2H_{BE}$, as illustrated in Fig. 1b).

are calculated. The expression of K is non-dimensionalized using the averaged time concentrations as follows:

$$K = \frac{\langle c \rangle}{\langle c_o \rangle} \tag{1}$$

where angular brackets $\langle\ \rangle$ denote the time average, $\langle c \rangle$ is the pollutant concentration and $\langle c_o \rangle$ the reference concentration given by:

$$\langle c_o \rangle = \frac{Q_e}{U_H H_{BE}^2 10^{-6}} \tag{2}$$

where U_H is the wind velocity at the roof height of the BE building in [m s^{-1}], H_{BE} is the height of the BE building in [m] and Q_e is the pollutant emission rate in [m^3 s^{-1}].

The average error over all samplers is evaluated by the following equation:

$$e_a = \frac{1}{N} \sum_{i=1}^{N} \left| \frac{K_{i,num} - K_{i,exp}}{K_{i,exp}} \right| \tag{3}$$

with N defined as the total number of the concerned samplers (here N is equal to 15 as can be seen in Fig. 6 where all samplers are clearly illustrated), $K_{i,num}$ and $K_{i,exp}$ represent the concentration measured numerically and experimentally at each sampler, respectively.

Fig. 4 shows the evolution of the average error, e_a, of K as a function of sampling time. The average error over all samplers is calculated at each 0.1 second and during a sampling time of 4 s. The distribution of e_a presents high fluctuations, in the first range of 2 seconds, mainly due to the transient period. Thereafter, a strong decrease of these fluctuations occurs throughout the following one second period. Finally, between 2.9 and 4 seconds, a clear stabilisation of the average error is established,

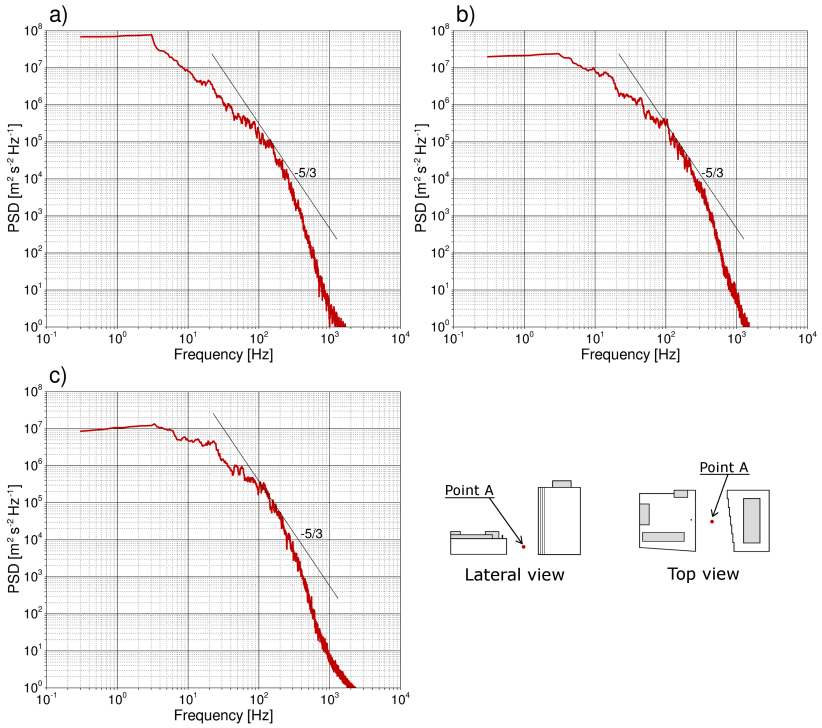

Figure 3: Power spectral density of velocity components in (a) streamwise, (b) spanwise, and (c) vertical directions, recorded at point A located in the centreline between the two buildings and at half-height of the BE building from the ground (i.e. $y = 0$ m, $x = 5H_{BE}$ and $z = 1/2H_{BE}$, as illustrated in Fig. 1b).

therefore a statistical averaging period of 3.5 s is judged sufficient for obtaining statistically-steady mean values, which correspond to a full-scale averaging time of about 12 minutes. Consequently, the non-dimensional concentrations over such a statistical averaging period are presented in this paper.

4. Results and validation

In this section, detailed results obtained with the DES turbulence model are described and compared to both RNG and wind tunnel results [34] to highlight the differences between the two modelling approaches (i.e. steady-state RNG and unsteady-state DES models). Firstly, the comparison focuses mainly on the mean concentration K values for the various results available from the wind tunnel experiments for the case selected and studied ($h_s = 1$ m and $M = 5$). Afterwards, other parameters such as flow-field structures and Reynolds stress components ($\langle u_i' u_j' \rangle$) are compared between DES and RNG approaches.

The basic strategy of LES is to resolve most of the turbulent kinetic energy, k, of the flow and modelling most of the dissipation ϵ [66], and this possible separation arises from the fact that k is determined by the large scales of motion and ϵ by the small scales [53]. In addition, LES approach is well known to be superior to RANS when validating flow fields and turbulence structures against experimental results [67]. Since (i) the 11 million cells grid is rigorously made by considering the Taylor-microscale resolution [52] and uses stretching ratios equal to 1 near walls and to 1.1 elsewhere, and (ii) the RLZ model is used for modelling the subgrid scales, known as one of best model among those of RANS $k - \epsilon$ models [68], one can consider that DES results are at least comparable to those that could be obtained with LES approach using the traditional Smagorinsky model which remains in wide use [69]. Consequently, since no wind-flow field data is available from the experimental results, the use of DES results as the reference for the aim of comparison to RANS is justified.

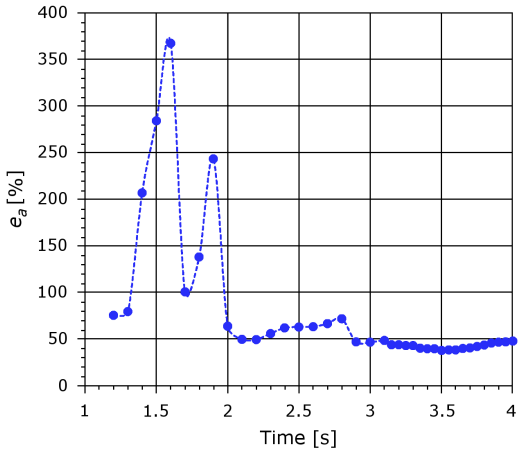

Figure 4: Average error between measured and calculated K over all samplers for time sampling between 1.2 and 4 seconds obtained with the case of $h_s = 1$ m and $M = 5$.

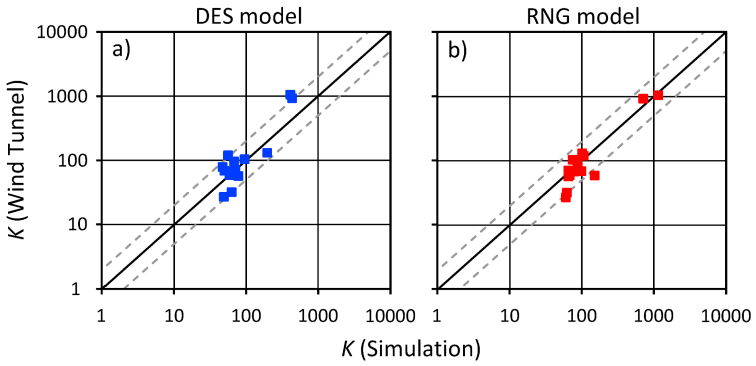

Figure 5: Scatter plots of simulation and wind tunnel K data obtained for the case of $h_s = 1$ m and $M = 5$ with (a) DES and (b) RNG models.

4.1. Average error of sampler concentrations

Fig. 5 compares the dispersion of K values on the BE roof and the top of the tower leeward wall between wind tunnel and CFD simulation results obtained at different samplers (detailed sampler locations for the studied case are shown in Fig. 6). Good agreement with experimental concentrations is shown by RNG model at the top of the tower leeward wall samplers compared to DES model whereas both DES and RNG simulations showed approximately the same dispersion of K over the BE building roof. The average error, e_a, provided by DES and RNG was 37% and 38%, respectively. These values illustrate the insignificant difference between the two tested models – further commented and discussed in this paper, while the required simulation time is 30 times greater when using DES approach. The dashed lines on each side of the median line indicate the limit of values located within a range factor of 2. Eighty percent (80%) and 86% of the DES and RNG concentration K values are within that portion, respectively. However, the correlation coefficient R of the dispersion K values is 0.96 for DES model and 0.97 for RNG model.

4.2. Concentrations on the BE building roof and top of Faubourg tower leeward wall

Fig. 6 shows the concentration K values at different samplers located on the BE building roof and on the top of the tower leeward wall obtained with both numerical approaches and wind tunnel experiments. As noted previously through Fig. 5a, the DES model showed significant underestimation

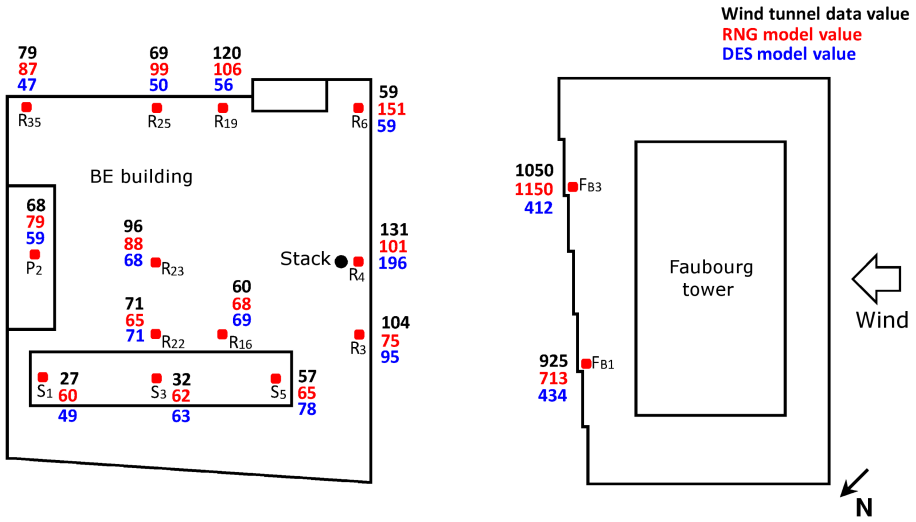

Figure 6: Simulation and wind tunnel values of K for $h_s = 1$ m and $M = 5$.

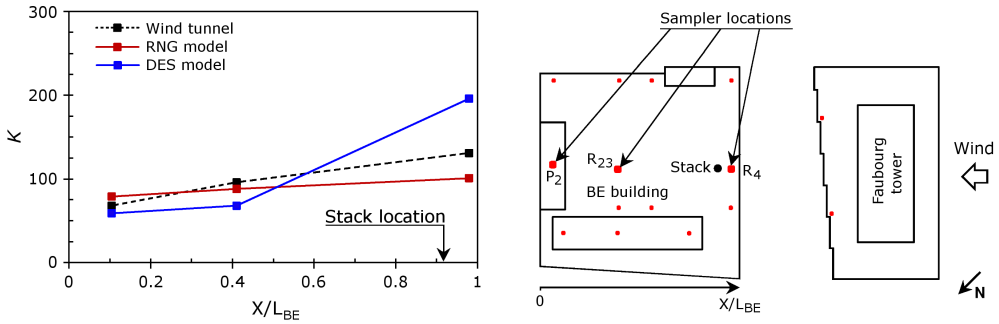

Figure 7: Measured and calculated variation of K at samplers R_4, R_{23} and P_2 along x axis on BE building roof for $h_s = 1$ m and $M = 5$.

of K values at samplers (F_{B1} and F_{B3}) of the tower leeward wall compared to those obtained by the RNG model whereas the trend of simulation results obtained on the BE building roof varies from one sampler to the other. Along the central line of the building roof, the RNG model shows better capability to approach the experimental values as detailed in Fig. 7; only at sampler P_2, located far in the back of the roof, DES approach has shown approximately the same result as RNG model. On the lateral samplers of the roof, the RNG model remains the best representation of the wind tunnel values at samplers R_{35}, R_{19} and S_5 as can be seen in Fig. 6 whereas at samplers R_{25} and S_1, DES yields better results. At samplers R_3 and R_6 located near the building upwind wall, DES shows better concordance with wind tunnel results.

4.3. Concentrations along the Faubourg tower leeward wall

Fig. 8 indicates the vertical distribution of concentrations K along the leeward wall of the Faubourg tower. The results displayed for RNG model and wind tunnel experiments are obtained with $h_s = 3$ m and $M = 4.5$ whereas those shown for DES model are obtained with $h_s = 1$ m and $M = 5$. Lateb et al. [70] have studied the effect of stack height and pollutant exhaust velocity using the same two-building configuration. The authors have concluded that increasing the momentum ratio M with a small stack height h_s is similar than reducing the momentum ratio for higher h_s and conversely, especially on the leeward wall of the Faubourg tower and the windward wall of the BE building. Therefore, the

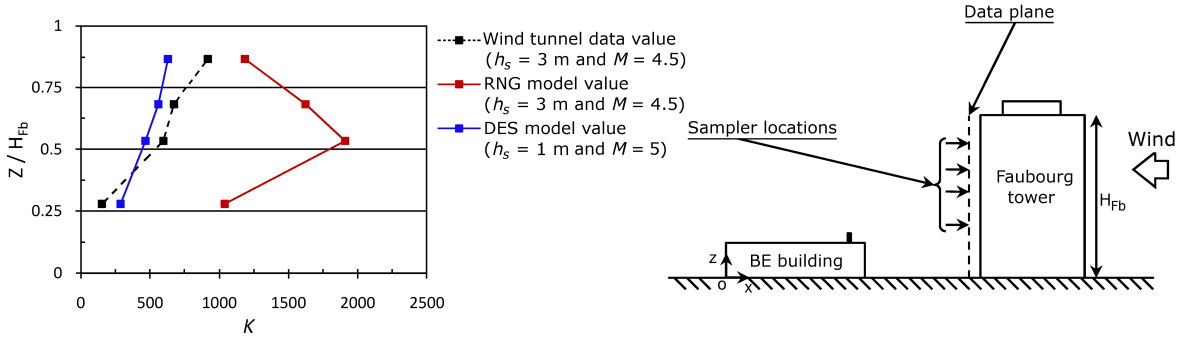

Figure 8: Vertical profiles of K on leeward wall of the Faubourg tower (Wind tunnel and RNG simulation values for $h_s = 3$ m and $M = 4.5$, and DES simulation values for $h_s = 1$ m and $M = 5$).

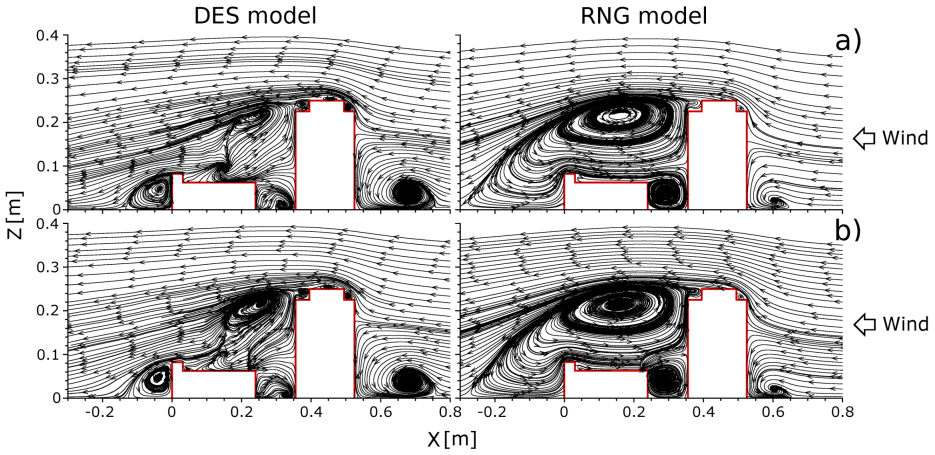

Figure 9: Vertical (x-z) plane distribution of streamlines by time averaged velocity for the case of $h_s = 1$ m and $M = 5$ through (a) the centre of the domain ($y = 0$ m) and (b) the stack position ($y = 0.0155$ m).

comparison between these two cases ($h_s = 1$ m with $M = 5$ and $h_s = 3$ m with $M = 4.5$) is intended to assess the vertical evolution of the concentrations using DES model since the case of $h_s = 3$ m and $M = 4.5$ was not considered in this study. The DES model results show good agreement with wind tunnel results, while the RNG model values overestimate clearly the experimental results. The vertical trend of K distribution is well reproduced by DES compared to RNG, which shows an opposite trend in the upper region.

As partial deduction for this section of results, DES shows the same average error (37%) compared to RNG model (38%), while RNG provides better distribution of K values. At most samplers (F_{B1}, F_{B3}, R_4, R_{19}, R_{23}, R_{35} and S_5), RNG has produced closer results to experiment, whereas DES model provides better concordance with experimental values only at few samplers (R_{22}, R_3 and R_6). DES results depicted in Fig. 8 agreed well with the wind tunnel results along the Faubourg tower leeward wall while the RNG model overestimated significantly the experimental K values along the tower leeward wall.

5. Analysis and discussion

5.1. Flow field analysis

Fig. 9 shows the streamlines by time averaged wind velocities in the vertical (x-z) plane through the stack position and the centreline of the domain. The well-known horseshoe vortex system [63, 6]

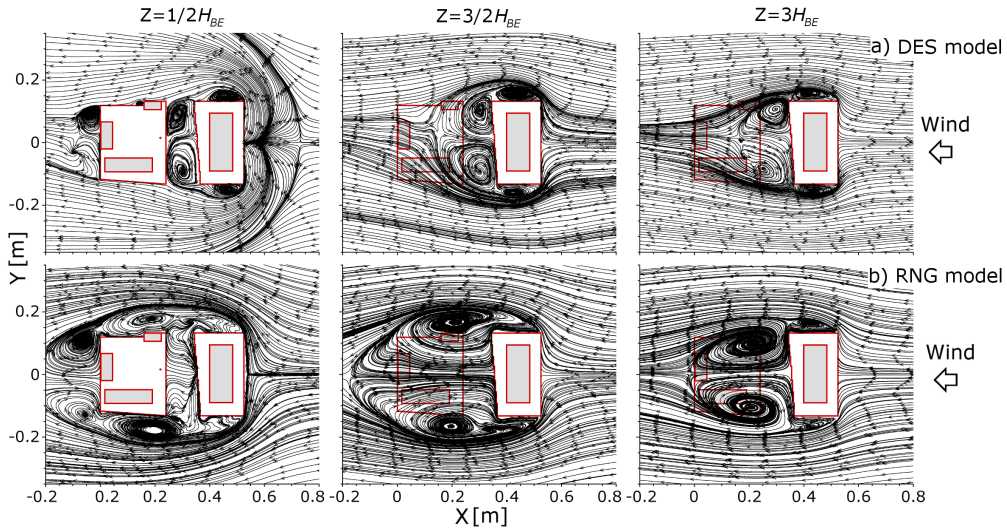

Figure 10: Horizontal (x-y) plane distribution of streamlines by time averaged velocity at different vertical positions for the case of $h_s = 1$ m and $M = 5$ obtained with (a) DES and (b) RNG models. Columns from left to right represent the results at height $z = 1/2H_{BE}$, $z = 3/2H_{BE}$ and $z = 3H_{BE}$ from the ground, respectively.

induced by the airflow pattern around the tower is well established in the upwind part of the tower – as shown in Fig. 9 by the vortex in front of the tower – with DES compared to RNG which displayed a very small horseshoe vortex. Two other vortices are apparent for DES, one between the two buildings and another in the BE building wake, while RNG showed only the recirculation zone between the two buildings. However the other recirculation zone behind the BE building is included in the recirculation zone induced by the tower roof. In other words, the recirculation region generated by the tower roof was so extended that it reached the BE building wake, thus forming only one single recirculation zone in the vertical plane behind the Faubourg tower, as shown in Fig. 9 for RNG model.

In order to gain an insight about the length of the recirculation zone behind the Faubourg tower, the recirculation cavity length, L_r, of the latter was evaluated using the approximate equation ($L_r = B_S^{0.67} B_L^{0.33}$) recommended for use by ASHRAE [14]; where B_S is the smaller of the tower upwind face dimensions (height or width) and B_L is the larger. The length L_r evaluated for the two-building configuration of interest is about 0.24 m. The RNG model shows clearly in Fig. 9 an overestimation of L_r value (= 0.6 m), while DES exhibits a complex recirculation zone, without borders clearly delimited. However, at height $z = 3/2H_{BE}$ of the horizontal plan shown in Fig. 10a, an approximate recirculation length of 0.25 m is observed. In addition, this overestimation issue of recirculation region behind a building when using RANS models has been already stated by several authors (e.g. [31, 32, 71, 72]). According to Yoshie et al. [72], this overestimated reattachment length is mainly due to the steady-state approach of RANS models which did not reproduce the vortex shedding behind the tower. Consequently, very large velocities in streamwise direction are induced by the reversed flow [32].

When analysing the streamlines in the vertical plane passing by the stack presented in Fig. 9b, the exhausted pollutant velocity appears less disrupted by the wind flow above the stack with DES than does the RNG, because of the higher pollutant emission velocity ($M = 5$). Indeed, for RNG the pollutant is directed towards the tower leeward wall immediately when it expelled from the stack, while with DES the pollutant rose in height then directed towards the tower leeward wall. This could partly explain the correct approach of the concentration by RNG at samplers F_{B1} and F_{B3} – previously noticed in Fig. 6 – which is just a consequence of the overestimated recirculation zone that, in turn, resulted from the steady-state approach of the RNG model, as previously explained.

Recently Nozu and Tamura [73] have noted that using RANS models results in very high concentrations, particularly when the source emission is located in the wake zone. This observation is clearly

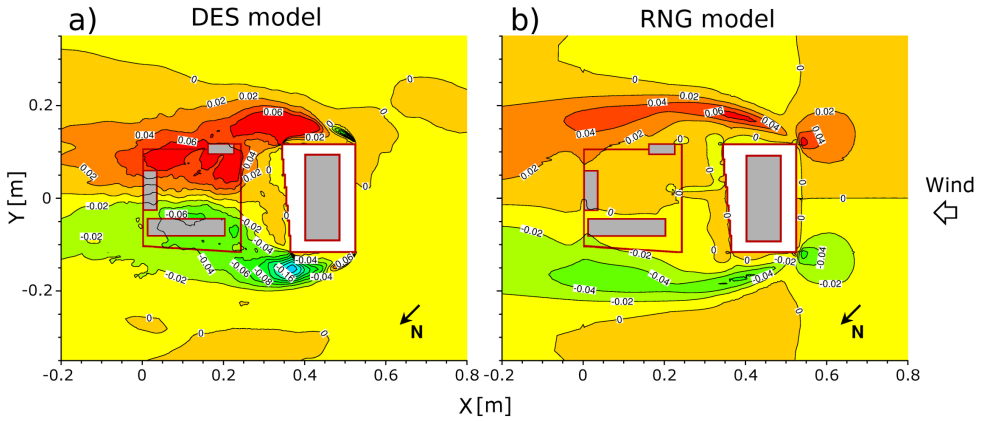

Figure 11: Distribution of non-dimensional shear stress component $\langle u_1' u_2' \rangle / U_H^2$ iso-contours on the horizontal plane (x-y) at height $z = 3/2H_{BE}$ for the case of $h_s = 1$ m and $M = 5$ with (a) DES model and (b) RNG model.

illustrated in Fig. 8 since the distribution of K in the vertical direction along the tower leeward wall is quite overestimated. However, for DES modelling, the reversed flow interacting with the transient vortices and the tower leeward wall boundary forms a free shear layer, and fluctuated periodically because of Kelvin-Helmholtz-type instability [74]. In additional, the Reynolds number of 2.5×10^4 – based on the BE building height – remains an important mixing parameter for flows in which the shear layers arising from separation of the boundary layers at the salient edges [75], like those of the staircase shape of the tower leeward wall. Consequently, the pollutant carried by the reversed flow from the stack is well mixed and transported laterally. This could also explain the good agreement of K at samplers R_3 and R_6 shown in Fig. 6 and along the vertical direction of the tower leeward wall presented in Fig. 8.

Fig. 10 shows the streamlines by time averaged wind velocities in the horizontal (x-y) plane at different vertical heights from the ground ($z = 1/2H_{BE}$, $3/2H_{BE}$ and $3H_{BE}$). The horseshoe phenomenon is well shown by DES through the horizontal plane ($z = 1/2H_{BE}$) in Fig. 10a. At higher levels ($z = 3/2H_{BE}$ and $3H_{BE}$) shown in Fig. 10, two main vortices are clearly distinguished in the Faubourg tower wake for both models. Vortices illustrated by RNG in Fig. 10b appear more symmetrical than those depicted by DES; while the vortices configuration presented in Fig. 10a for DES simulations showed a northwest side vortex more significant than that of the southeast side. This is due to the difference in width between the two tower sides. Consequently, the wind-flow field produced by DES has better taken into account the horizontal staircase form of the tower leeward wall than RNG, which can be explained by the vortex shedding reproduced by DES but not with the RNG approach.

Despite the good agreement in concentration values between the RNG model and experimental results, at the BE roof samplers in general and at the top of the tower leeward wall samplers (i.e. F_{B1} and F_{B3}) in particular, three main anomalies are apparent in the wind-flow field analysis: (i) significant overestimation of the recirculation zone length in the tower wake, (ii) non-consideration of the difference in width between the tower sides, and (iii) insignificant reproduction of the horseshoe phenomenon in the upstream part of the tower in spite of the strong wind-flow velocity. In principle, the lack of all these basic flow characteristics around an obstacle like the Faubourg tower indicates that the wind-flow structure has not been well simulated by RNG as opposed to DES which seems to reproduce the wind-flow configuration far better.

5.2. Distribution of shear stress components

The horizontal movement of the vortex shedding towards the lateral directions is mainly fulfilled by $\langle u_1' u_2' \rangle$ and $\langle u_2' u_2' \rangle$ shear stress components in the tower wake region. Therefore, Fig. 11 depicts the

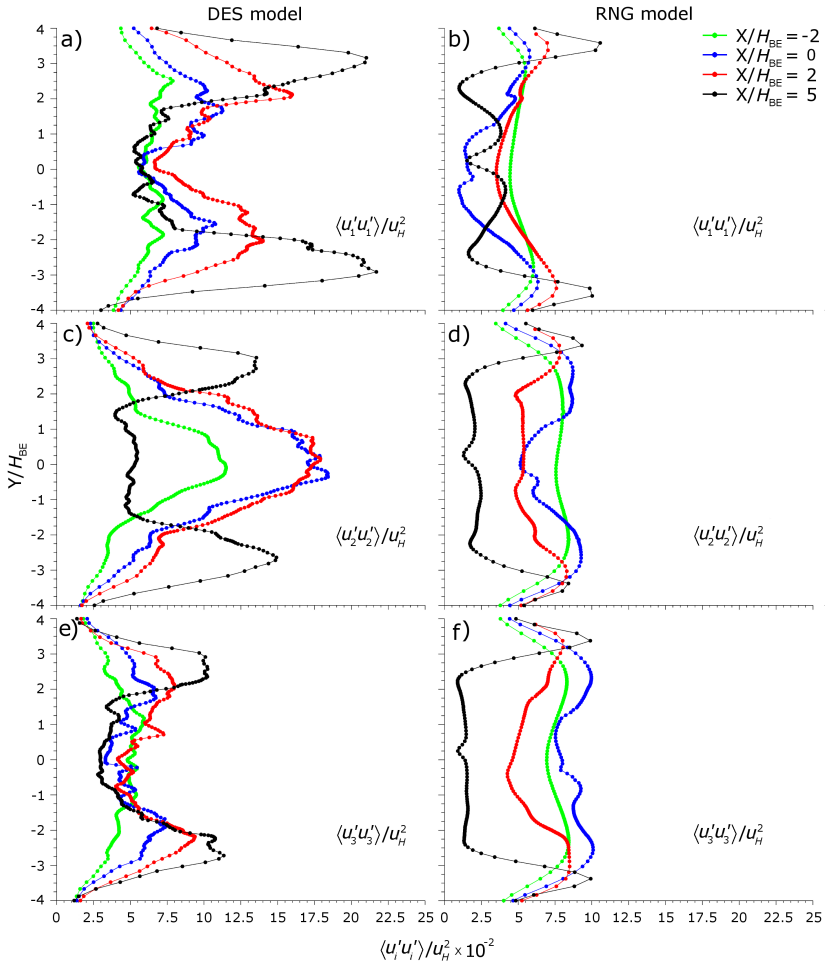

Figure 12: DES- and RNG-based distribution of non-dimensional Reynolds normal stress components ($\langle u_i' u_i' \rangle / U_H^2$) along horizontal lines at $z = 3/2H_{BE}$ and for four streamwise positions (i.e. $x/H_{BE} = -2$, 0, 2 and 5, as illustrated in figure 1b).

horizontal distribution of non-dimensional shear stress component $\langle u_1' u_2' \rangle / U_H^2$ at height $z = 3/2H_{BE}$ to assess the vortex shedding production behind the tower. Note that the modelled part of $\langle u_1' u_2' \rangle$ values is less significant than those of the resolved part, nevertheless the non-dimensional values presented in Fig. 11 are estimated as the algebraic sum of the two parts ($\langle u_1' u_2' \rangle_{res} + \langle u_1' u_2' \rangle_{SGS}$) when using DES. The distribution of $\langle u_1' u_2' \rangle / U_H^2$ values shows clearly the vortices induced by the Faubourg tower sides, directed towards the central plane when following the absolute value of 0.04 and 0.02 with DES, see Fig. 11a. In contrast to the RNG approach shown in Fig. 11b, the absolute value of 0.04 remains outside the wake region, and the movement of vortices of which the absolute value is of 0.02 begins heading towards the central plane at the end of the extended wake region. The distribution between the northwest and the southeast leeward wall corners of the tower is clearly different for DES with significant absolute values of $\langle u_1' u_2' \rangle / U_H^2$ at the northwest leeward corner, while the distribution presented by RNG is rather similar at both tower leeward wall corners. This confirms the non-consideration of the horizontal staircase form of the tower leeward wall stated previously.

Figs. 12 and 13 show the distribution of the Reynolds normal stress components $\langle u_i' u_i' \rangle$ normalized by U_H^2 along the horizontal and vertical lines, respectively, located at four streamwise positions (i.e. $x/H_{BE} = -2$, 0, 2 and 5 as illustrated in Fig. 1b). Horizontal lines are in plane (x-y) at height $z =$

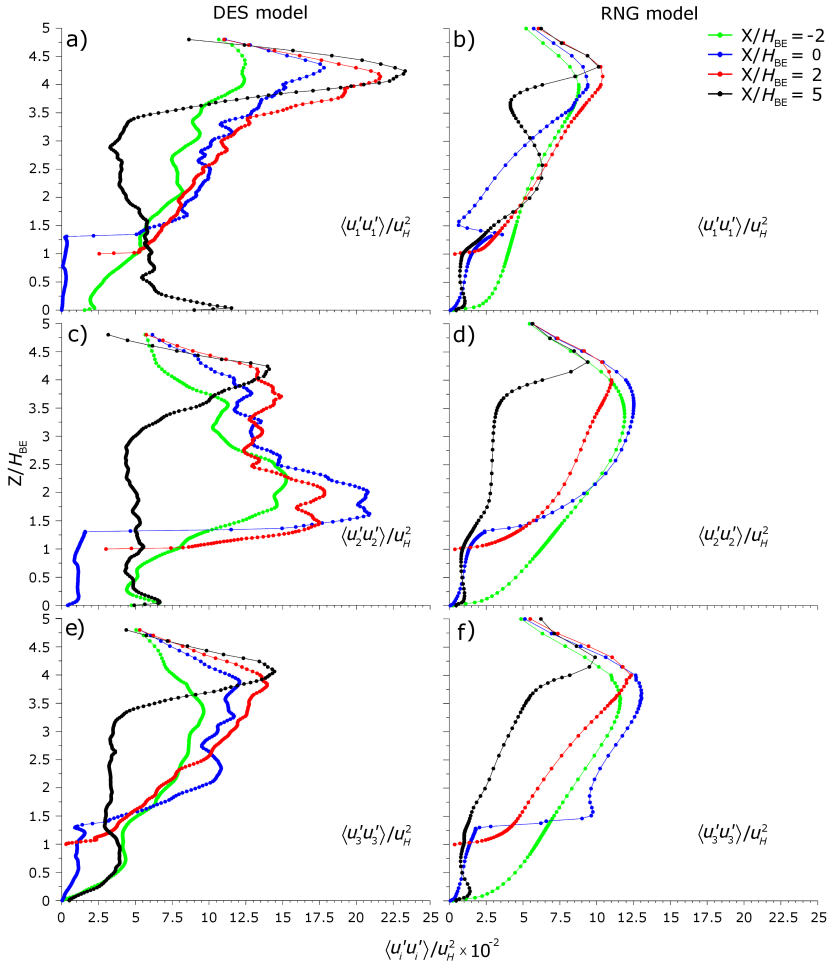

Figure 13: DES- and RNG-based distribution of non-dimensional Reynolds normal stress components ($\langle u_i' u_i' \rangle / U_H^2$) along vertical lines in the central plane ($y = 0$) and for four streamwise positions (i.e. $x/H_{BE} = -2$, 0, 2 and 5, as illustrated in Fig. 1b).

$3/2H_{BE}$ and vertical lines are contained in the central plane ($y = 0$). For the RNG model, all non-dimensional component values vary between 0 and 0.125, while for DES the variation range lies within 0 and 0.235. The trend between the three $\langle u_i' u_i' \rangle$ components is almost the same for RNG model when comparing with DES results which, in turn, show significant difference in the Reynolds normal stress component distributions. However, the streamwise component $\langle u_1' u_1' \rangle$ distributions, in vertical and horizontal lines at the BE building leeward wall (i.e. $x/H_{BE} = 0$) shown in Figs. 12b and 13b with RNG, present small values because of the reversed flow and the lateral movements which occurred in that region (see Figs. 9a and 10b), and therefore promote the lateral and vertical components $\langle u_2' u_2' \rangle$ and $\langle u_3' u_3' \rangle$ as shown in Figs. 12 and 13. In region above the BE building behind the tower (i.e. $x/H_{BE} = 0$ and 2), the DES model showed very large values of $\langle u_2' u_2' \rangle$ component compared to $\langle u_1' u_1' \rangle$ and $\langle u_3' u_3' \rangle$ as can be seen in Figs. 12c and 13c.

In many regions of the flow-field structure, the RNG model shows large values of $\langle u_i' u_i' \rangle$ compared to DES. For instance, in the lower part along the vertical leeward wall of the BE building (i.e. $x/H_{BE} = 0$), the RNG model exhibits large $\langle u_1' u_1' \rangle$ values compared to those of DES (see Fig. 13a and b). This results from large velocities stated previously in the streamwise direction when using the RNG model. Far in the wake zone at side regions of the BE building (i.e. $x/H_{BE} = -2$ and 0), the lateral, $\langle u_2' u_2' \rangle$,

and vertical, $\langle u_3' u_3' \rangle$, components are also very large with RNG compared to those of DES as can be seen in Fig. 12c–f.

These observations reveal that the lateral momentum diffusion is insufficient so that it is impossible to reproduce correctly the tower wake region, and thus to accurately evaluate its reattachment length when using the RNG model. In addition, the anisotropy of the Reynolds normal stress components – that may be associated with the highly intermittent character of the wake region flow [16, 71] – has been well taken into account by DES, whereas the RNG model has not considered it sufficiently. In other words, on the one hand, the underestimation and/or overestimation of the Reynolds stress components, when using the RNG approach, results in an incorrect reproduction of the flow-field structure. On the other hand, the steady-state methodology of RNG does not favour the vortex shedding production, therefore the lateral diffusion is highly underestimated especially in the immediate wake region.

Finally, the steady-state RANS methodology, in general, cannot predict the turbulent pollutant transport process accurately since the dispersion field is closely related to flow-field behaviour [33]. Nonetheless, one can say that RNG model remains an acceptable approach to estimate concentration values for dispersion where advection transport phenomena dominate – like over the BE roof region – while for regions where the turbulent diffusion process is more significant – like within the immediate wake zone behind the tower – DES model performs best. Since it is not always evident to identify in advance the advection transport dominate regions, the reader is cautioned on the use of RANS models in inappropriate circumstances. Given the sampler positions considered in this study, one can argue that the agreement between RNG and wind tunnel measurements may be particular to this configuration where a lower building (BE building) set immediately downstream of a taller building (Faubourg tower) has stabilized the flow to a certain extent.

6. Conclusions

In the present work, the dispersion of pollutants around a two-building configuration has been investigated using the unsteady-state detached-eddy simulation approach, and the results have been compared to steady-state RNG $k-\epsilon$ model as well as experimental wind tunnel data. The purpose is to evaluate the effects of the unsteadiness and the Reynolds stress component anisotropy in reproducing the flow and dispersion fields when comparing between DES and RNG approaches. The main findings of the study can be summarized as follows.

In terms of the flow field, DES approach seems to reproduce correctly the recirculation zone in the wake region, while the RNG model has clearly overestimated the recirculation region. The horseshoe vortex system induced by the airflow pattern around the upstream tower is well established with DES compared to RNG model. The vortex shedding induced by the tower sides in the wake region is not reproduced properly by RNG whereas this phenomenon is clearly observed with DES.

In terms of pollutant dispersion, both models show approximately the same average error of concentrations calculated over all samplers. For concentration values at samplers F_{B1} and F_{B3} located at the top of the tower leeward wall, the RNG model shows better agreement with experimental values compared to DES. This good agreement is likely due to the large streamwise velocities in the reversed flow that are a consequence of the steady-state methodology of RNG model [32]. However the DES model reproduces with good agreement the distribution of concentrations in the vertical direction along the tower leeward wall, while the RNG approach exhibits a significant overestimation.

The underestimation and/or overestimation of Reynolds stress components and the steady-state methodology of RNG $k-\epsilon$ model tend, respectively, to (i) distort and/or limit the Reynolds stress component values, and (ii) not reproduce contribution of periodic fluctuation due to the transient characteristics of the flow field, particularly in wake regions where high anisotropy is exhibited. Consequently, RANS approaches are generally unable to reproduce the wind-flow structure and the pollutant transport process accurately.

In terms of central processing unit (CPU) time, the DES model required approximately 30 times more computing time than the RNG model. Given the similar average errors of concentration obtained by the DES and RNG approaches, the steady-state RNG model remains an approach that can be used

and trusted for obtaining an insight into the dispersion process at specific measurement points where dispersion is mainly dominated by the advection transport phenomenon. Finally, the DES model seems to indicate that the unsteady-state approach is more appropriate to reproduce the physics of the flow-field development as well as the concentration field.

Acknowledgements

Financial support for this study from the *Fonds Québécois de la Recherche sur la Nature et les Technologies* (*FQRNT*) is gratefully acknowledged. The first author would like to thank Dr. Mourad Yataghene for fruitful discussions and helpful comments. The authors express their great appreciation to the reviewers for their insightful comments and very helpful suggestions for improvements. A sincere acknowledgement is given to Prof. Dr. Robert N. Meroney, emeritus professor at Colorado State University, for his invaluable comments based on his long personal experience in computational and experimental wind engineering.

References

[1] V. D. Assimakopoulos, H. M. ApSimon, N. Moussiopoulos, A numerical study of atmospheric pollutant dispersion in different two-dimensional street canyon configuration, Atmos. Environ. 37 (29) (2003) 4037–4049.

[2] C. Mockett, F. Thiele, Overview of detached-eddy simulation for external and internal turbulent flow applications, In: *Proceedings of the Fifth Intl Conf. on Fluid Mechanics*, Shanghai, China, 2007.

[3] G. Easom, Improved turbulence models for computational wind engineering, PhD thesis, School of Civil Engineering, University of Nottingham, England, 2000.

[4] C. H. Chang, R. N. Meroney, Numerical and physical modeling of bluff body flow and dispersion in urban street canyons, J. Wind Eng. Ind. Aerod. 89 (14–15) (2001) 1325–1334.

[5] E. Sterling, Overview of detached-eddy simulation for external and internal turbulent flow applications, In: *Proceedings of the Symp. on Indoor Air Quality*, San Carlos de Bariloche, Argentina, 1988.

[6] B. Blocken, T. Stathopoulos, J. Carmeliet, J. L. M. Hensen, Application of computational fluid dynamics in building performance simulation for the outdoor environment: an overview, J. Building Perform. Simul. 4 (2) (2011) 157–184.

[7] M. Schatzmann, B. Leitl, J. Liedtke, Dispersion in urban environment; comparison of field measurements with wind tunnel results, Environ. Monit. Assess. 65 (1–2) (2000) 249–257.

[8] S. C. Morris, S. R. Stolpa, P. E. Slaboch, J. C. Klewicki, Near-surface particle image velocimetry measurements in a transitionally rough-wall atmospheric boundary layer, J. Fluid Mech. 580 (2007) 319–338.

[9] W. W. Li, R. N. Meroney, J. A. Peterka, Wind-tunnel study of gas dispersion near a cubical model building, Report to Site Safety Research Branch, Office of Nuclear Regulatory Research, Washington D.C. (Report: CER81-82WWL-RNM-JAP8), Colorado State University, USA, 1981.

[10] W. W. Li, R. N. Meroney, Gas dispersion near a cubical model building: part I. Mean concentration measurements, J. Wind Eng. Ind. Aerod. 12 (1) (1983a) 15–33.

[11] W. W. Li, R. N. Meroney, Gas dispersion near a cubical model building: part II. Concentration fluctuation measurements, J. Wind Eng. Ind. Aerod. 12 (1) (1983b) 35–47.

[12] R. J. Brown, R. W. Bilger, An experimental study of a reactive plume in grid turbulence, J. Fluid Mech. 312 (1996) 373–407.

[13] J. Y. Vincont, S. Simoëns, M. Ayrault, J. M. Wallace, Passive scalar dispersion in a turbulent boundary layer from a line source at the wall and downstream of an obstacle, J. Fluid Mech. 424 (2000) 127–167.

[14] ASHRAE, Chapter 44: Building air intake and exhaust design, in: Ashrae handbook – Heating, ventilating, and air-conditioning applications, American Society of Heating, Refrigerating and Air-conditioning Engineers (ASHRAE), Atlanta, USA, 2007.

[15] B. Hajra, T. Stathopoulos, A wind tunnel study of the effect of downstream buildings on near-field pollutant dispersion, Build. Environ. 52 (2012) 19–31.

[16] H. S. Kang, C. Meneveau, Passive scalar anisotropy in a heated turbulent wake: new observations and implications for large-eddy simulations, J. Fluid Mech. 442 (2001) 161–170.

[17] D. Banks, R. N. Meroney, R. L. Peterson, J. J. Carter, Evaluation of Fluent for predicting concentrations on buildings, In: *Proceedings of the Annual Meeting of the Air and Waste Management Association* (AWMA), San Diego, CA, USA, 2003.

[18] O. Coceal, A. Dobre, T. G. Thomas, S. E. Belcher, Structure of turbulent flow over regular arrays of cubical roughness, J. Fluid Mech. 589 (2007) 375–409.

[19] G. Brethouwer, E. Lindborg, Numerical study of vertical dispersion by stratified turbulence, J. Fluid Mech. 631 (2009) 149–163.

[20] D. A. Philips, R. Rossi, G. Iaccarino, Large-eddy simulation of passive scalar dispersion in an urban-like canopy, J. Fluid Mech. 723 (2013) 404–428.

[21] L. Campos-Arriaga, Wind energy in the built environment: a design analysis using CFD and wind tunnel modelling approach, PhD thesis, University of Nottingham, England, 2009.

[22] EPA, Guideline on air quality models, *United State Environmental Protection Agency* (EPA), (EPA-450/2-78-027), Research Triangle Park, NC, USA, 1978.

[23] W. H. Snyder, Guideline for fluid modeling of atmospheric diffusion, United State Environmental Protection Agency (EPA), *Tech. Rep.* (EPA-600/8-81-009), Research Triangle Park, NC, USA, 1981.

[24] R. N. Meroney, Guidelines for fluid modeling of dense gas cloud dispersion, J. Hazard. Mater. 17 (1) (1987) 23–46.

[25] AIAA, Guide for the verification and validation of computational fluid dynamics simulations, *American Institute of Aeronautics and Astronautics* (AIAA), VA. AIAA-G-077 (ISBN: 1-56347-285-6), Reston, VA, USA, 1998.

[26] W. L. Oberkampf, T. G. Trucano, Verification and validation in computational fluid dynamics, Prog. Aerosp. Sci. 38 (3) (2002) 209–272.

[27] J. Franke, A. Hellsten, H. Schlünzen, B. Carissimo, Best practice guideline for the CFD simulation of flows in the urban environment, *Cost Action 732*, 2007.

[28] Y. Tominaga, A. Mochida, R. Yoshie, H. Kataoka, T. Nozu, M. Yoshikawa, T. Sharasawa, AIJ guidelines for practical applications of CFD to pedestrian wind environment around buildings, J. Wind Eng. Ind. Aerod. 96 (10–11) (2008) 1749–1761.

[29] AIAA, Guide to reference and standard atmosphere models, *American Institute of Aeronautics and Astronautics* (AIAA), (ISBN: 978-1-60086-784-2), Reston, VA, USA, 2010.

[30] J. Franke, A. Hellsten, H. Schlünzen, B. Carissimo, The Cost 732 best practice guideline for CFD simulation of flows in the urban environment: a summary, Intl J. Environ. Pollut. 44 (1–4) (2011) 419–427.

[31] W. Rodi, Comparison of LES and RANS calculations of the flow around bluff bodies, J. Wind Eng. Ind. Aerod. 69–71 (1997) 55–75.

[32] N. G. Wright, G. J. Easom, Non-linear $k-\epsilon$ turbulence model results for flow over a building at full-scale, Appl. Math. Model. 27 (12) (2003) 1013–1033.

[33] Y. Tominaga, T. Stathopoulos, Numerical simulation of dispersion around an isolated cubic building: comparison of various types of $k-\epsilon$ models, Atmos. Environ. 43 (20) (2009) 3200–3210.

[34] M. Lateb, C. Masson, T. Stathopoulos, C. Bédard, Comparison of various types of $k-\epsilon$ models for pollutant emissions around a two-building configuration, J. Wind Eng. Ind. Aerod. 115 (2013a) 9–21.

[35] S. M. Salim, Computational study of wind flow and pollutant dispersion near tree canopies, PhD thesis, Division of Environment, University of Nottingham Malaysia Campus, Malaysia, 2011.

[36] P. R. Spalart, W. H. Jou, M. Strelets, S. R. Allmaras, Comments on the feasibility of LES for wings, and on a hybrid RANS/LES approach, In: *Advances in DNS/LES*, Ed. C. Liu and Z. Liu, Columbus, OH: Greydon Press, 137–147., 1997.

[37] M. Shur, P. R. Spalart, M. Strelets, A. Travin, Detached-eddy simulation of an airfoil at high angle of attack, In: *Engineering Turbulence Modelling and Experiments 4*, Ed. W. Rodi, D. Laurence, Oxford, Elsevier Sci., 669-678., 1999.

[38] P. R. Spalart, Young-person's guide to detached-eddy simulation grids, *Tech. Rep.* NASA/CR-2001-211032, NASA, 2001.

[39] P. R. Spalart, Topics in detached-eddy simulation, In: *Proceedings of the Conf. on Computational Fluid Dynamics*, Ed. V. Springer, 2004.

[40] P. R. Spalart, K. D. Squires, The status of detached-eddy simulation for bluff bodies, In: *Direct and Large-eddy simulation*, pp. 29–45., 2004.

[41] D. Basu, A. Hamed, K. Das, DES and hybrid RANS/LES models for unsteady separated turbulent flow predictions, In: *Proceedings of the 43th AIAA Aerospace Sciences Meeting and Exhibit*, Pap. No. AIAA-2005-0503, Reno, NV, USA, 2005.

[42] S. Deck, Zonal-detached-eddy simulation of the flow around a high-lift configuration, AIAA J. 43 (11) (2005) 2372–2384.

[43] U. Bunge, C. Mockett, F. Thiele, Guidelines for implementing detached-eddy simulation using different models, Aerosp. Sci. Technol. 11 (5) (2007) 376–385.

[44] S. Deck, P. E. Weis, M. Pamiès, E. Garnier, On the use of simulated detached-eddy simulation (SDES) for spatially developing boundary layers, In: *Advances in Hybrid RANS/LES*, Ed. S.-H. Peng and W. Haase, 2008.

[45] P. R. Spalart, Detached-eddy simulation, Annu. Rev. Fluid Mech. 41 (2009) 181–202.

[46] S. E. Haupt, F. J. Zajaczkowski, L. J. Peltier, Detached-eddy simulation of atmospheric flow about surface mounted cube at high Reynolds number, J. Fluids Eng. 133 (3) (2011) 1–8.

[47] S. Deck, Recent improvements in the zonal-detached-eddy simulation (ZDES) formulation, Theor. Comp. Fluid Dyn. 26 (6) (2012) 523–550.

[48] T. Stathopoulos, L. Lazure, P. Saathoff, A. Gupta, The effect of stack height, stack location and rooftop structures on air intake contamination: a laboratory and full-scale study, *Institut de recherche Robert-Sauvé en santé et en sécurité du travail* (IRSST/Report-392), Montreal, Canada, 2004.

[49] B. Caruelle, F. Ducros, Detached-eddy simulations of attached and detached boundary layers, Intl J. Comput. Fluid D. 17 (6) (2003) 433–451.

[50] M. Lateb, C. Masson, T. Stathopoulos, C. Bédard, Detached-eddy simulation of pollutant dispersion around an urban two-building configuration, 12th Americas Conference on Wind Engineering 2013, ACWE 2013: Wind Effects on Structures, Communities, and Energy Generation vol. 1 (ISBN: 978-162993065-7) (2013b) p. 641–653, Seattle, WA, USA.

[51] P. R. Spalart, S. Deck, M. L. Shur, K. D. Squires, M. K. Strelets, A. Travin, A new version of detached-eddy simulation, resistant to ambiguous grid densities, Theor. Comp. Fluid Dyn. 20 (3) (2006) 181–195.

[52] Q. Liao, E. A. Cowen, Relative dispersion of a scalar plume in a turbulent boundary layer, J. Fluid Mech. 661 (2010) 412–445.

[53] H. Tennekes, J. L. Lumley, A first course in turbulence, The MIT Press, 1972.

[54] M. Lateb, C. Masson, T. Stathopoulos, C. Bédard, Numerical simulation of pollutant dispersion around a building complex, Build. Environ. 45 (8) (2010) 1788–1798.

[55] R. Kraichnan, Diffusion by a random velocity field, Phys. Fluids 13 (1) (1970) 22–31.

[56] R. Smirnov, S. Shi, I. Celik, Random flow generation technique for large-eddy simulations and particle-dynamics modeling, J. Fluids Eng. 123 (2) (2001) 359–371.

[57] J. C. H. Fung, J. C. R. Hunt, N. A. Malik, R. J. Perkins, Kinematic simulation of homogeneous turbulence by unsteady random Fourier modes, J. Fluid Mech. 236 (1992) 281–318.

[58] R. C. Maple, Adaptive harmonic balance method for unsteady, nonlinear, one-dimensional periodic flows, PhD thesis, Department of the air force, Air Force Institute of Technology, Ohio, USA, 2002.

[59] S. V. Patankar, D. B. Spalding, A calculation procedure for heat, mass and momentum transfer in three-dimensional parabolic flows, Intl J. Heat Mass Tran. 15 (10) (1972) 1787–1806.

[60] P. Gousseau, B. Blocken, G. J. F. van Heijst, CFD simulation of pollutant dispersion around isolated buildings: on the role of convective and turbulent mass fluxes in the prediction accuracy, J. Hazard. Mater. 194 (2011) 422–434.

[61] P. Gousseau, B. Blocken, G. J. F. van Heijst, Large-eddy simulation of pollutant dispersion around a cubical building: analysis of the turbulent mass transport mechanism by unsteady concentration and velocity statistics, Environ. Pollut. 167 (2012) 47–57.

[62] R. Courant, K. Friedrichs, H. Lewy, On the partial difference equations of mathematical physics, IBM J. Res. Dev. 11 (2) (1967) 215–234.

[63] Z. Liu, Y. Xiong, Z. Wang, S. Wang, Numerical simulation and experimental study of the new method of horseshoe vortex control, J. Hydrodyn. 22 (4) (2010) 572–581.

[64] M. Lateb, Numerical study of near-field pollutant dispersion around a building complex emitted from a rooftop stack, PhD thesis, Department of Mechanical Engineering, École de technologie supérieure (Éts), Montreal, Canada, 2013.

[65] K. D. Squires, Detached-eddy simulation: current status and perspectives, In: *Direct and Large-eddy simulation V*, Ed. R. Friedrich, B J. Geurt and O. Métais, pp. 465–480, Kluwer Academic Publishers., 2004.

[66] D. Fröhlich, J. von Terzi, Hybrid LES/RANS methods for the simulation of turbulent flows, Prog. Aerosp. Sci. 44 (2008) 349–377.

[67] Y. Tominaga, T. Stathopoulos, CFD modeling of pollution dispersion in building array: evaluation of turbulent scalar flux modeling in RANS model using LES results, J. Wind Eng. Ind. Aerod. 104–106 (2012) 484–491.

[68] B. Blocken, T. Stathopoulos, P. Saathoff, X. Wang, Numerical evaluation of pollutant dispersion in the built environment: comparisons between models and experiments, J. Wind Eng. Ind. Aerod. 96 (10–11) (2008) 1817–1831.

[69] J. O'Neil, C. Meneveau, Subgrid-scale stresses and their modelling in a turbulent plane wake, J. Fluid Mech. 349 (1997) 253–293.

[70] M. Lateb, C. Masson, T. Stathopoulos, C. Bédard, Effect of stack height and exhaust velocity on pollutant dispersion in the wake of a building, Atmos. Environ. 45 (29) (2011) 5150–5163.

[71] T. Shirasawa, R. Yoshie, H. Takana, T. Kobayashi, A. Mochida, Y. Endo, Cross comparison of CFD results of gas diffusion in weak wind region behind a high-rise building, In: *Proceedings of the 4th Intl Conf. on Advances in Wind and Structures* (AWAS'08), Jeju, Korea, 2008.

[72] R. Yoshie, G. Jiang, T. Shirasawa, J. Chung, CFD simulations of gas dispersion around high-rise building in non-isothermal boundary layer, J. Wind Eng. Ind. Aerod. 99 (4) (2011) 279–288.

[73] T. Nozu, T. Tamura, LES of turbulent wind and gas dispersion in a city, J. Wind Eng. Ind. Aerod. 104–106 (2012) 492–499.

[74] T. Hasama, S. Kato, R. Ooka, Analysis of wind-induced inflow and outflow through a single opening using LES & DES, J. Wind Eng. Ind. Aerod. 96 (10–11) (2008) 1678–1691.

[75] H. C. Lim, I. P. Castro, R. P. Hoxey, Bluff bodies in deep turbulent boundary layers: Reynolds-number issues, J. Fluid Mech. 571 (2007) 97–118.